Numerical Elucidation of Flow and Dispersion in Ordered Packed Beds: Non-Spherical Polygons and the Effect of Particle Overlap on Chromatographic Performance

Numerical Elucidation of Flow and Dispersion in Ordered Packed Beds: Non-Spherical Polygons and the Effect of Particle Overlap on Chromatographic Performance

Fabian Dolamore[1*], Simone Dimartino[2] and Conan J. Fee[1,3]

[1]Biomolecular Interaction Centre, [3]School of Product Design, University of Canterbury, Private Bag 4800, Christchurch, New Zealand 8041

[2]Institute for Bioengineering, School of Engineering, The University of Edinburgh, Edinburgh EH9 3FB, UK

Corresponding Author

*E-mail: fabian.dolamore@canterbury.ac.nz
Phone: +6427 728 2030

ABSTRACT: Spherical particles are widely considered as the benchmark stationary phase for preparative and analytical chromatography. Although this has proven true for randomly packed beds in the past, we challenge this paradigm for ordered packings, the fabrication of which are now feasible through additive manufacturing (3D printing). Using computational fluid dynamics (Lattice Boltzmann Method) this work shows that non-spherical particles can both reduce mobile-phase band broadening and increase permeability compared with spheres in ordered packed beds. In practice, ordered packed beds can only remain physically stable if the particles are fused to form a contiguous matrix, thus creating a positional overlap at the points of fusion between what would otherwise be discrete particles. Overlap is shown to decrease performance of ordered packed beds in all observed cases, thus we recommend it should be kept to the minimum extent necessary to ensure physical stability. Finally, we introduce a metric to estimate column performance, the mean deviated velocity, a quantitative description of the spread of the velocity field in the column. This metric appears to be a good indicator of mobile-phase dispersion in ordered packed bed media, including overlapped beds and is a useful tool for screening new stationary phase morphologies without having to perform computationally expensive simulations.

Recent computational studies have demonstrated that ordered sphere packings can improve chromatographic performance compared with random packing[1,2]. This is caused by the homogenous distribution of path lengths along which the mobile phase is transported through ordered media. These theoretical studies are now gaining practical relevance because ordered stationary phases can be fabricated using additive manufacturing technologies or three-dimensional printing[3-5]. 3D printing offers a high level of control over the morphology of fabricated micro-structures, thus facilitating the translation of ordered packings from the virtual environment to practical implementation in real chromatographic systems[6-8].

Spherical beads have been shown to have better chromatographic performance when compared to irregular particles in randomly packed beds[9]. This was a result of more homogenous porosity distribution in packings of spherical particles, which increased the heterogeneity of the random flow channels and reduced eddy dispersion. Comparatively, ordered beds of spherical particles are homogeneous by design and inherently reduce eddy dispersion effects[1,2,10,11]. Because ordered packings do not require the homogeneity that spherical particles provide in random packings, we question the superiority of spherical particles in the context of ordered packed beds.

When studying ordered packed beds, several geometric factors become manipulatable and important. Using computational fluid dynamics (CFD), it has been shown that the configuration of spherical particles, namely: simple cubic (SC), body centred cubic (BCC) and face centred cubic (FCC) has marked impact on the chromatographic performance of ordered packed beds comprising mono-disperse spheres[1,2]. Moreover, we have shown that the orientation of the axial flow direction with respect to the packed bed, described using miller indices: [001], [011] and [111], changes the reduced plate height while not affecting the permeability of the same spherical packed beds[1].

Preceding this work, practical residence time distribution experiments have been performed using 3D printed stationary phases comprising various uniform particle shapes[8]. Interestingly, beds of tetrahedral particles were characterized with lower mobile phase dispersion (measured by plate height, *HETP*), than their spherical counterparts, a result attributed to a reduced variance of the axial velocity in the flow channels as well as smaller volume of stagnation zones. On the topic of packed beds of non-spherical particles, Li et al. computationally predicted that ellipsoidal particles produce lower band broadening than spheres in SC and BCC arrangements[12], further questioning the use of spherical particles in ordered stationary phases. In the context of randomly packed beds, Schure and Maier recently proposed that ellipsoidal particles can alleviate

the negative impact of wall effects in confined packed beds, thus reducing band broadening in practical chromatographic media[13].

In practice, ordered beds of packed particles are susceptible to physical instability because of the high void spaces and limited contact between particles. Movement of particles from their intended locations can be caused by pressure and shear forces from the flow of the mobile phase or during column handling, thus resulting in a defective lattice. The simplest way to maintain bed integrity in 3D printed beds is to design a certain overlap between the particles, effectively merging them into a continuous and rigid structure[8,14] resembling a monolithic support rather than a bed packed with discrete particles.

We use CFD to study the performance of ordered packed beds with respect to four design variables, namely: i) bed configuration, ii) bed orientation, iii) particle shape and iv) particle overlap. and use these findings to gain a greater understanding of how packed bed geometry affects fluid flow and solute dispersion. Because the number of possible permutations when manipulating these four variables was beyond our computational resources, we only studied structures discussed in previous work, and those able to be created through 3D printing, i.e. spherical, octahedral and tetrahedral particles. These data sets were then used to draw general conclusions on the influence of the bed morphology and velocity profile on chromatographic performance.

Experimental and Numerical Methods

Computation Fluid Dynamics. The Lattice Boltzmann Method (LBM) was used to simulate fluid flow and solute dispersion in these systems, as described previously[1]. Briefly, Palabos (open source C++ Library and LBM solver developed by FlowKit Ltd., Lausanne, Switzerland) was used to solve the fundamental equations of the LBM. Velocity fields were resolved to laminar equilibrium using the Bhatnagar–Gross–Krook (BGK) collision operator[15] on a D3Q19 lattice using a spatial resolution of 30 nodes per particle. The relaxation parameter, τ, was constrained to unity, as per literature recommendations for porous media systems[16].

Propagation of an inert solute tracer pulse in the advection-convection lattice was simulated by a modified single relaxation time model[17], also using a D3Q19 lattice and relaxation time of unity. Periodic boundary conditions were employed in the transverse directions on both lattices, representing a stationary phase of infinite width, thus neglecting wall effects[18,19]. The inlet boundary was defined as a Dirichlet condition for both lattices, representing a constant uniform inlet velocity for the flow lattice and a variable inlet concentration of the inert tracer for the advection-diffusion lattice, facilitating simulation of a "pulse" injection at the packing inlet, mirroring practical chromatographic practices[20]. The outlet of both lattices was defined as a Neumann outflow.

Packed Bed Design. A hierarchy of parameters is employed in this study to illustrate and distinguish between the different ordered beds considered. At the top of the hierarchy are the morphological features over which we have direct control, i.e. bed configuration, bed orientation, particle shape and overlap (Fig. 1). On the second level of the hierarchy are the resulting structural parameters, namely characteristic length and porosity, which are directly determined by the selection of the morphological variables. Velocity is the main independent variable representing the operating conditions employed in the simulations, which can be expressed in non-dimensional coordinates in terms of the Peclet number. Finally, the reduced plate height, permeability and separation impedance are the performance metrics that describe the packed bed's ability to perform a chromatographic separation and thus enable us to compare the geometries considered.

To distinguish between morphologies in this work, we employ a notation that covers each of the four independent morphology variables. For example, SC [001] $S_{\lambda=1}$ represents a simple cubic (SC) configuration with orientation [001] of spheres (S) with a contiguity value of 1. Each of these four terms is explained in the following section. It is important to note that the flow direction refers to the cartesian 'Z' dimension for all cases in this work.

Morphological Features. In the context of packed bed design, these are the features over which we have direct control. Configuration refers to how particles are arranged with respect to each other within the packed bed. We focus on three configurations: simple cubic (SC), body-centred cubic (BCC) and face-centred cubic (FCC) (Fig. 1a), which are analogous to the configurations found in the cubic crystal system[21]. These systems have been studied by several authors[1,2,12].

Orientation describes how the packed bed aligns with the axial flow direction. Three orientations are explored here, as denoted by their Miller index notation, where [001], [011] and [111] identify the plane normal to the superficial velocity vector through the medium (Fig. 1b). This variable can be conceptualized as a rotation of the packed bed by $\pi/4$ in the YZ plane for the [011] orientation and a further $\tan^{-1}(1/\sqrt{2})$ in the XZ plane for the [111] orientation. We have explored this concept in our previous work and shown that it has a marked impact on system band broadening while maintaining a constant pressure drop, a useful finding for optimizing chromatographic systems[1].

Particle shape describes the geometry of the individual particles that comprise the packed bed. We compare three particle shapes in this work, spheres (S), octahedra (O) and tetrahedra (T) (Fig. 1c) based on the work of Nawada et al.[8], who found experimentally that these alternative shapes (O and T) can produce equal, if not lower, band broadening than spherical particles in ordered packed beds.

Some of the packing configurations explored in this work involve overlapping particles, which would impart mechanical stability to the ordered bed (Fig 1d). The degree of overlap is measured using the contiguity factor, λ, defined as the ratio between the porosity of the packing, ε, and the porosity of a reference state, ε_{ref}:

$$\lambda = \frac{\varepsilon_{ref}}{\varepsilon} \quad (1)$$

where the reference state is the closest possible packing of discrete particles for the given morphology, i.e. their faces are touching but not overlapping. Accordingly, the contiguity for beds with overlapping particles will be $\lambda > 1$, while $\lambda < 1$ describes ordered expanded beds. While flow properties of hypothetical static expanded beds of particles have been previously been investigated in the literature[22], this case is not attainable practically. The contiguity factor here defined employs the bed porosity for its evaluation, a parameter that is readily available for chromatographic beds, thus making its calculation simple.

Structural Parameters. These variables characterise a designed bed morphology, but do not directly describe the suitability of the medium for chromatographic purposes. Here, we consider three variables: characteristic length and porosity.

The characteristic length, d, is a key estimator of the length scale of the resulting packed bed. The particle diameter, or averaged equivalent, is the parameter of choice for many preceding works[1,2,12,23,24]. However, such characteristic length cannot be easily generalized to other shapes than spherical particles, let alone to more complex monolithic beds with overlapping particles. In addition, band broadening effects are associated with mass transfer and mixing phenomena occurring in the mobile phase. For these reasons, we considered the hydraulic diameter, d_h, defined as the ratio of void volume to surface area, as a characteristic length to compare the different geometries[25]:

$$d_h = \frac{\varepsilon V}{SA} \tag{2}$$

where V [L^3] is the volume of the unit cell and SA [L^2] is the surface area of the unit cell. Key to interpreting this work is understanding that the non-dimensionalized data presented herein is independent of the particle size – i.e. particles of any size produce identical van Deemter curves, assuming that the Stokes Flow condition is maintained (Re < 1) and a consistent definition of d is employed. Thus, the absolute hydraulic diameter value itself is not important, rather the ratio between the particle size and the hydraulic diameter - which is of course constant. Hence, for clarity we report the normalized hydraulic diameter, $\hat{d}_h = d_h/d_p$ (where d_p for each shape is the unit cell edge length illustrated in Fig. 1c).

Porosity, ε, is the ratio of the void space (occupied by the mobile phase) to the total volume of the medium:

$$\varepsilon = \frac{V_{void}}{V_{tot}} \tag{3}$$

where V_{void} [L^3] is the fluid volume of the medium and V_{tot} [L^3] is the total volume of the medium. Porosity is often considered as an indicator of permeability in packed beds through empirical relationships such as the Carman-Kozeny equation (CKE) and the Ergun equation[26,27]. The Peclet number (reduced velocity), Pe, is the ratio of advective to diffusive transport of a chemical species in solution:

$$Pe = \frac{d\hat{u}}{D} \tag{4}$$

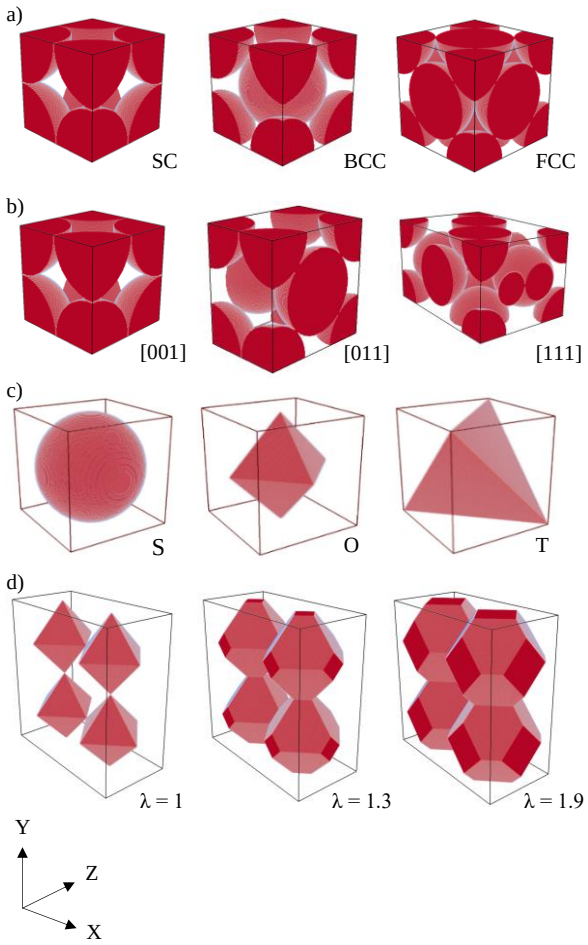

Figure 1. Illustration of the four morphological features that were controlled in this study a) particle configuration and b) bed orientation (shown for SC only), c) particle shape and d) contiguity (shown using octahedra, for clarity). Z is the axial flow direction.

where d [L] is the characteristic length scale, $\hat{u}$ [LT^{-1}] is the average channel velocity and D [L^2T^{-1}] is the molecular diffusion coefficient of the solute in the mobile phase. This parameter is regularly employed to non-dimensionally describe chromatographic systems, most notably in the van Deemter equation[20].

Performance Metrics. The performance metrics used to compare bed configurations are the Darcy Number, Da[28], reduced plate height, h[29], and separation impedance, E [30] (all dimensionless). These metrics are widely used to characterize the performance of real chromatography columns[31], thus allowing for comparison between simulated and physical packed columns. The Darcy number is a dimensionless form of permeability, as defined by Darcy's law[32].

$$Da = \frac{k}{d^2} = -\frac{v\,\mu}{d^2}\frac{dL_Z}{dP} \tag{5}$$

where k [L^2] is the permeability, v [LT^{-1}] is the superficial velocity, μ [$ML^{-1}T^{-1}$] is the fluid viscosity, and dL_z/dP [$M^{-1}L^2T^2$] is the inverse of the axial pressure gradient.

Dispersion behaviour was quantified by the reduced plate height, h, which describes the ratio of increase in the variance of a solute peak, σ^2 [T^2], to the mean elution time, t [T]. Δ is used to represent the difference between two sampling points within the medium, thus we do not have to assume that the pulse input is represented by a Dirac function – which would be an accurate assumption in our simulated environment.

$$h = \frac{\Delta\sigma^2}{(\Delta t)^2} \cdot \frac{l}{d} \quad (6)$$

where l [L] is the axial distance between the two sampling points. A more detailed explanation of this methodology can be found in our previous work[1]. In this work, h_{min} corresponds to the lowest observed value of h for a specified packing. This was taken as the lowest h value of the simulated data points.

Separation Impedance, E, is a combination of the other two performance metrics and considers the importance of both solute dispersion and bed permeability[30]. When optimizing a porous medium, E should be minimized, representing a porous medium with low solute dispersion and high permeability. This metric is also useful for analysis of porous media because it does not require definition of a characteristic system length (as can be shown by substituting Eq. 5 and 6 into Eq. 7), which can often be an ambiguous choice.

$$E = \frac{h^2 \varepsilon}{Da} \quad (7)$$

Results and Discussion

Particle Shape. Spheres have previously been shown to reduce eddy dispersion when compared with irregular particles in randomly packed beds, by homogenizing flow channel size and length[9]. However, it is unknown if this correlation holds for ordered packed beds. To investigate this, octahedral and tetrahedral particles were compared with their spherical counterparts in the SC, BCC and FCC configurations in each of the defined orientations: [001], [011] and [111] (except FCC octahedra, which do not form permeable flow channels in any orientation).

It has been demonstrated previously that the CFD model accurately predicts permeability data for random and ordered packings of mono-disperse spherical particles[1]. Furthermore, as was the case for spherical particles, the *Da* values of the media created by non-spherical polygons were found to be independent of the orientation of the bed, hence only one value is reported in Table 1.

Because spherical particles minimize surface area, and thus drag forces, non-spherical polygons of equivalent volume may be expected to decrease permeability within an ordered porous medium of equivalent structure. Our model supports this theory for the SC arrangement, however, for BCC and FCC spheres show the lowest *Da* value (Table 1), suggesting that there are further factors that contribute to flow resistance in packed beds (as discussed later in this section).

The best tetrahedral and octahedral packings not only outperform their spherical counterparts for h_{min}, but also achieve this optimum at a higher Peclet number (Fig. 2). This is especially beneficial for reducing band broadening of large molecules such as proteins, which have small diffusion coefficients, because these species are usually subjected to much higher Peclet numbers in applications such as fast protein liquid chromatography (FPLC).

Table 1. Flow characteristics of each particle shape in each of the studied configurations. No overlap (λ = 1) for all packings reported.

Shape	*Config.*	$\hat{d}_h$	ε	*Da* ×10^{-3}
S	SC	0.61	0.48	7.2
	BCC	0.32	0.32	5.1
	FCC	0.23	0.26	3.2
O	SC	1.92	0.82	5.8
	BCC	0.77	0.62	6.8
T	SC	0.77	0.66	5.6
	BCC	0.86	0.72	7.2
	FCC	1.29	0.81	6.6

Naturally, these results raise the question as to why non-spherical packed beds would have superior performance to spherical particles in ordered systems, when this is not the case for randomly packed beds. A major difference between random and ordered packings is how particles are arranged. In random packing, particle shape directly affects the conformation of the packed bed because particles align randomly. Randomly aligned non-spherical particles may result in widely varying channel geometries that could include occluded regions of the bed where flat-face interactions between neighbouring particles occur. Such variations do not occur with spherical particles because of their rotational similarity. In ordered packings, particle location and alignment are predetermined, meaning that the geometry of the flow channels is always uniform.

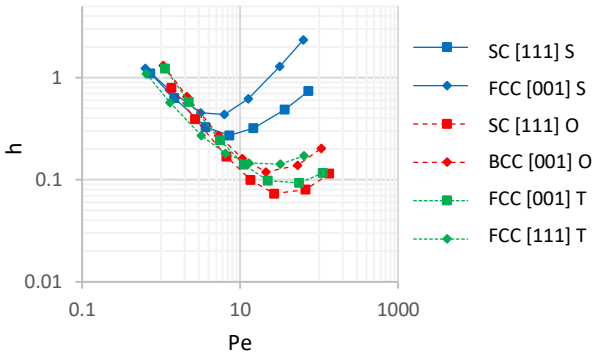

Figure 2. The two best performing arrangements of each particle shape are presented here with no overlap (λ = 1). For the full data set, refer to Fig. S4.

Consider the simplest case, the SC [001] morphology, for each particle shape and the respective velocity profile within the unit cell (Fig. 3). For spherical particles, the streamline profiles show a high proportion of flow in the bottom quartile of velocity magnitude. This is caused by the narrow flow restrictions in

spherical packs that create a "squeezing" effect on the flow channels. This directly contributes mass transfer resistance by decreasing the homogeneity of the velocity field and explains how solute dispersion is increased as per van Deemter's plate height model[29]. Furthermore, we suggest that this is an important influence on the system *Da*, because drag force in a fluid is proportional to the square of velocity. Therefore, channels with more uniform flow profiles will have higher permeability when compared to channels that oscillate between expansion and contraction.

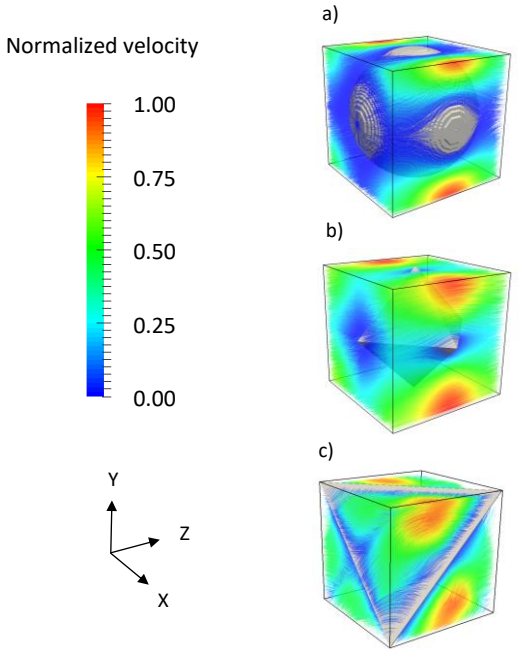

Figure 3. Streamlines representing normalized profiles through the unit cell for each particle shape: a) sphere, b) octahedron and c) tetrahedron in the SC [001] arrangement with no overlap ($\lambda = 1$). Z is the axial flow direction. Velocities are normalized by the maximum channel velocity. Simulations are in the Stokes Flow Regime ($Re < 1$).

Particle Overlap. Although we know that particle overlap is necessary in physical ordered packed beds, to what extent it affects performance of these media is yet to be determined; an important consideration for practical application of particle overlap. In this work, overlap was defined by increasing the particle diameter without increasing the distance between particle centres, hence the contiguity value of each packing type responds uniquely to an increase in particle overlap and are not constant for each reported system. Furthermore, overlap was only investigated for a handful of packings: SC [all] S, SC [all] O and SC [001], BCC [001] and FCC [001] T, to reduce the size of the data set while still accurately observing the effect of overlap.

Because overlap directly impacts the porosity of a bed, it is expected that an increasing overlap would be correlated with decreased bed permeability. This is validated by our model, which shows that increased overlap resulted in smaller *Da* values for all observed morphologies (Table 2).

For all observed configurations, increasing overlap increased the reduced plate height of the medium, to differing degrees (Fig. 4a). To explain this, let us consider how overlap affects

Table 2. Flow characteristics for packings using overlap for all particle shapes studied in this work.

Shape	*Config.*	λ	$\hat{d}_h$	ε	$Da \times 10^{-3}$
S	SC	1.00	0.61	0.48	7.2
		1.26	0.43	0.38	4.7
		1.92	0.32	0.25	1.9
O	SC	1.00	1.92	0.82	5.8
		1.30	0.98	0.63	3.8
		2.10	0.59	0.39	2.0
T	SC	1.00	0.77	0.66	5.6
		1.33	0.52	0.50	4.5
		2.52	0.37	0.32	2.9
	BCC	1.00	0.85	0.72	7.2
		1.46	0.44	0.49	5.4
		3.05	0.23	0.24	1.6
	FCC	1.00	1.29	0.81	6.6
		1.30	0.69	0.63	7.1
		1.96	0.41	0.41	3.6

the pore structure of the bed. Increasing overlap does not alter the characteristic shape of flow channels, it only constricts them – resulting in a narrower channel profile. Hence, increasing particle overlap should not be expected to decrease mobile phase band broadening; this can only be a result of a morphology change. However, overlap will reduce the hydraulic diameter of the system as a result of the pore constriction, thus the magnitude of h_{min} increases even if the absolute plate height is constant. To further illustrate this, reduced kinetic plots[33] were produced using the same data sets (Fig. 4b). Because increasing λ decreases permeability by constricting the pore size, E can only increase when the absolute plate height is unaffected (note that it was previously discussed that E does not depend on the characteristic length). Furthermore, the agreement in performance heirachy between these two dimensionless analyses provides validation for our choice of using d_h as the length scale for analysing ordered porous media.

This performance decrease for increasing overlapped beds is an important result for 3D-printed ordered packed beds in practice, because it suggests that when considering mobile phase performance, particle overlap should always be minimized. To apply this knowledge in practice, a relationship between overlap and structural integrity should ideally be determined in the future for various particle shapes, materials and configurations. Such a relationship would allow for optimization of overlap to create a high strength packed bed with low band broadening.

It is important to note that the current work only considers band broadening in the mobile phase. In many real chromatographic systems, a permeable stationary phase also plays an important role in the separation process. Size exclusion media incorporate a porous stationary phase that provides internal tortuous flow paths that separate small molecules from larger ones

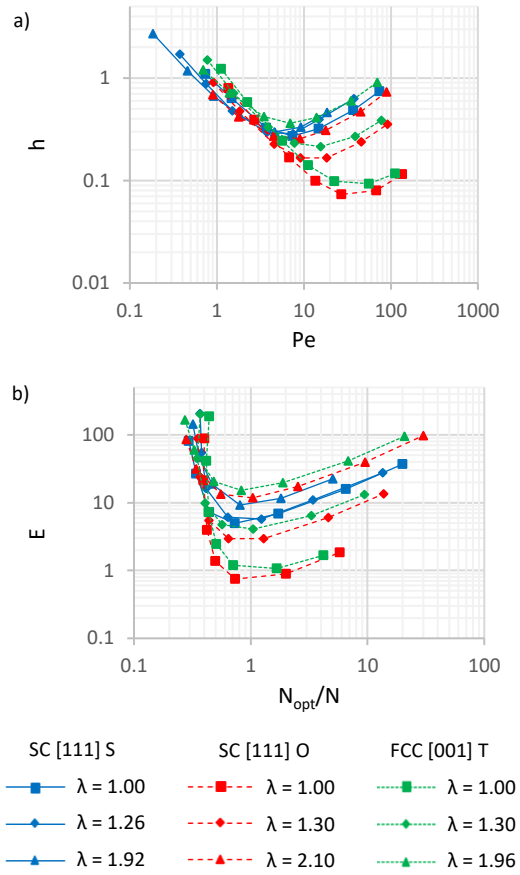

Figure 4. The effect of particle overlap on the best performing morphologies from each particle shape using two dimensionless analyses: a) reduced van Deemter curves and b) reduced kinetic plots. Particle overlap is represented by the contiguity factor, λ. Full sets of van Deemter plots are provided in the supporting information Fig. S6.

through differences in mobile-phase to stationary-phase partitioning and greater overlap may be beneficial to this process. Moreover, ion exchange and affinity-based media often use porosity in the stationary phase to increase surface area for binding substrate molecules. In such media, the stationary phase volume will influence the column capacity. Increasing the overlap would increase the stationary phase volume, meaning that column length could be reduced to achieve an equivalent capacity, reducing total band broadening. Conversely, increasing overlap will increase the path length of solute molecules within the stationary phase and contribute heavily to mass transfer resistance. These considerations are speculative and there is a large body of work that must be completed before real conclusions can be drawn about the extension of this study into more complex chromatographic systems.

Packed Bed Performance. Comparing the separation impedance (a function of *h* and *k*) with the porosity of a medium, we found no optimum structure that minimizes both separation impedance and porosity (Fig. 5) – though there is a general hierarchy of morphologies. Note that data from a fifth morphological variable, "rotation" (Section S2) is included to increase

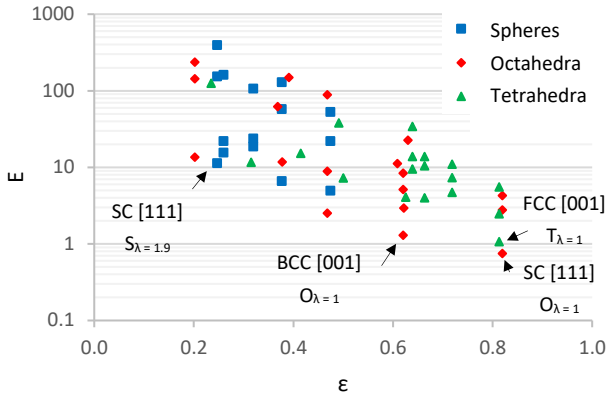

Figure 5. Separation Impedance vs. porosity for ordered packings of monodisperse particles. Three points exist at each porosity value, representing the three orientations of each structure. Only labels for structures with small impedance are reported, for clarity.

the sample size of the following analyses. Recommended morphologies are found along the bottom of the series, while points located above this have increasingly inferior performance. Because packings with $\lambda = 1$ are considered physically unstable, we draw attention to SC [111] S as a contender for best performing physically viable structure, as it performs well at higher Finding optimal solutions to improve column performance is non-trivial and may not be possible using current computing capabilities. The method that is employed in this work was essentially an optimization by trial and error. However, sampling a variety of morphologies provides insight into the favourable characteristics that reduce band broadening. To aid future optimization processes, we present two variables that appear to be good indicators of different aspects of chromatographic performance.

We propose that d_h^2 is strongly correlated with system permeability (Fig. 6). Linear regression analysis of packed beds with $\varepsilon > 0.3$ (blue squares), yields a gradient of $1/167$ ($R^2 = 0.99$), thus implying direct proportionality between these two variables.

$$k = \frac{{d_h}^2}{c} \tag{8}$$

where $c = 167$, which is similar to the Carman Kozeny constant (taken as 150 or 180 in the literature[34]). Substituting Eq. 8 into Eq. 5 (Darcy's law), yields an alternative to the CKE, for high porosity packed beds. This analysis implies that the Darcy number is near constant for packed beds where $\varepsilon > 0.3$.

$$\frac{dP}{dL_Z} = \frac{c\hat{u}\mu}{{d_h}^2} \tag{9}$$

Because the hydraulic diameter is defined as the ratio of void volume to surface area for a packed bed, it should not be surprising that it shows strong correlation to the system permeability. However, there is one major outlier for the high porosity data points (Fig. 6), SC $O_{\lambda=2.1}$, found below the general trend. This is thought to be a result of the narrow flow restrictions that

occur in this packed bed when compared to packed beds of similar porosity. These restrictions reduce system permeability by increasing the local velocity gradients. Furthermore, low porosity packings ($\varepsilon > 0.3$) deviate from this main trend (Fig. 6). These observations suggest that there is at least one other geometric factor has a significant effect on the permeability of a porous system, which becomes more influential at lower porosity. This factor is yet to be determined but is thought to be related to expansion and contraction of the axial flow channels through the medium.

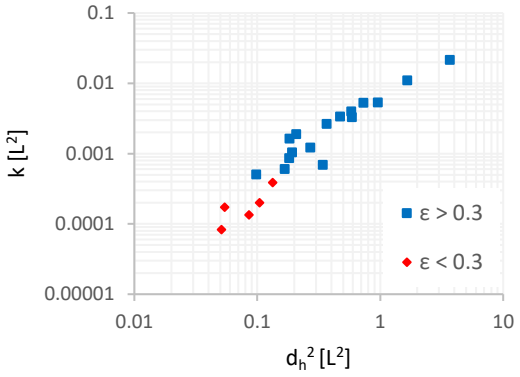

Figure 6. The relationship between hydraulic diameter and permeability for all packed beds studied in this work.

To estimate column performance we define here the normalized mean absolute deviation of the velocity field, u_{md}, which describes the variation in velocity across the pores of the media, which is the basis of mass transfer resistance ('C term') in van Deemter's plate height model (Fig. 7). We envision that, in the context of chromatography, an ideal porous media would have a uniform velocity profile, thus eliminating mass transfer resistance. Numerically, this is represented by a u_{md} value approaching zero.

$$u_{md} = \frac{\sum|u_i - \hat{u}|}{n\hat{u}} \qquad (10)$$

where u_i [LT^{-1}] is the velocity at a given simulation node in the unit cell and n is the number of simulation nodes. Thus, the numerator in Eq. 10 describes the sum of the differences between the local and average velocity at each simulation node, which is then normalized by the average velocity. We found that the data generated by the CFD model was better described using the mean deviation, rather than the standard deviation. Although the standard deviation is more commonly applied to data analysis, it is often found that the mean deviation is better for describing empirical data[35].

Though there is noticeable spread at higher values of, u_{md}, it does appear to be a strong indicator of minimum band broadening. This illustrates that media with more uniform channel velocity profiles experience less band broadening because the variance in advective transport across the pores is low. Because u_{md} can be calculated from the laminar velocity field of a medium, it does not require expensive dynamic CFD solution of the advection-diffusion equation. Hence, this metric could be used as a screening tool to eliminate structures that will have poor performance in our current hierarchy, allowing us to focus on examining more promising structures that score well with this metric.

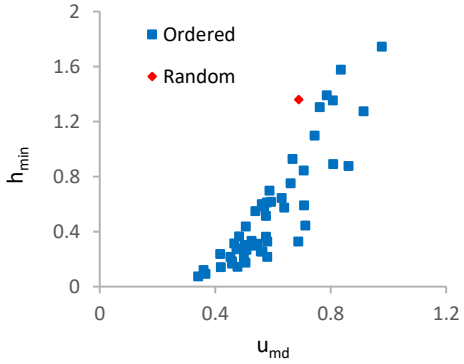

Figure 7. Estimating h_{min} using the normalized mean absolute deviation of the velocity field, for all morphologies studied in this work. The "Random" point in plot b) represents random close packing of mono-disperse spheres.

Interestingly, jammed random packing of spheres is a near outlier to this trend, producing an h_{min} value at the upper bound of the data set (Fig. 7). This illustrates the negative effect of eddy dispersion in randomly packed beds, caused by the variance of path lengths of the main channels that solute molecules must travel through. This analysis is a good starting point for advancing our understanding of porous systems and their practical applications. We suggest that there may be other factors relating to the structure of flow channels of a porous medium that have not been considered here that are important in this analysis, which will hopefully be discovered in future work.

Conclusions

In this study, we investigated the feasibility of using ordered non-spherical particles as a porous medium, specifically for use in practical chromatographic systems. This was achieved by comparing their performance with previously studied ordered spherical particle packings using common chromatographic metrics: permeability (Darcy number), reduced plate height and separation impendence.

We have shown that non-spherical particles in specific configurations can improve performance in ordered packed beds compared with their spherical analogues, further improving ordered packed beds in comparison to their random counterparts. It is suggested that this behaviour is caused by non-spherical solid shapes reducing the constriction effect on flow channels that is exhibited by spheres.

Because ordered packed beds are prone to physical instability, especially those with high porosity – the use of particle overlap is necessary to keep the packed bed stable and thus achieve consistent chromatographic performance. However, it was found that overlap increases both pressure and reduced plate height, making it detrimental to column performance in all

observed cases. We speculate, however, that overlap may be beneficial in cases of permeable solid-phase materials because it may increase column capacity by increasing the relative solid-phase volume.

We showed that system permeability is strongly correlated with hydraulic diameter. Furthermore, we found that optimum performance is strongly correlated with a new parameter, the mean average deviation of the velocity field. This is a useful tool that can act as an efficient computational screening in future studies, thus allowing us to exclude poor performing media from more detailed, and thus expensive, consideration. This is beneficial for optimization because solution of the laminar velocity field is less computationally expensive than a dynamic simulation of a tracer experiments to determine the reduced plate height of a medium.

The current work ignores wall effects by enforcing periodic boundary conditions in the CFD model. However, it is acknowledged that this is a major source of band broadening in ordered packed beds, which depends on both the column-to-particle diameter ratio and the dimensionless time scale. The impact of wall effects on band broadening are equally, if not more, important than the four packed bed variables introduced in this work. Quantification of wall effects in ordered packed beds and methods to minimize them are the focus of future publication.

As a final comment, the authors propose that the future of chromatographic media (especially when using 3D printing as a manufacturing method) lies in monolithic structures. This is because monolithic structures can be designed to have low (or zero) mean curvature, making their channels smooth for high permeability and more suited to production through additive manufacturing. Furthermore, monoliths have practically endless morphological permutations, thus there is far more design flexibility in the context of monoliths compared to predetermined particle shapes. Hence, when considering mobile phase band broadening, the design focus should be shifted from considering only the stationary phase morphology and toward optimal features of the macroscopic channels themselves.

Supporting Information

The supporting information for this work covers:

- Justification for the choice of characteristic length scale
- Particle Rotation - another novel degree of freedom in ordered packed beds
- Extended data sets for figures in the main text

Author Information

Corresponding Author

*E-mail: fabian.dolamore@canterbury.ac.nz
Phone: +6427 728 2030

ORCID

Fabian Dolamore: 0000-0001-5691-3448
Simone Dimartino: 0000-0002-9695-1278
Conan Fee: 0000-0002-3827-1039

Acknowledgement

This work was supported by funding from the Ministry of Business, Innovation and Employment (MBIE) of New Zealand (UOCX14 and UOCX15) and help and support from the Biomolecular Interaction Centre (BIC) and New Zealand eScience Infrastructure (NeSI).

References

(1) Dolamore, F.; Fee, C.; Dimartino, S. *J. Chromatogr. A* **2018**, *1532*, 150-160.
(2) Schure, M. R.; Maier, R. S.; Kroll, D. M.; Ted Davis, H. *J. Chromatogr. A* **2004**, *1031*, 79-86.
(3) Gaal, G.; Mendes, M.; de Almeida, T. P.; Piazzetta, M. H. O.; Gobbi, Â. L.; Riul Jr, A.; Rodrigues, V. *Sens. Actuators, B* **2017**, *242*, 35-40.
(4) Gibson, I.; Rosen, D.; Stucker, B. *Additive Manufacturing Technologies: 3D Printing, Rapid Prototyping, and Direct Digital Manufacturing*, 2nd 2015 ed.; Springer New York: New York, NY, 2015.
(5) Yang, Y.; Chen, Y.; Wei, Y.; Li, Y. *Int. J. Adv. Manuf. Technol.* **2016**, *84*, 2079-2095.
(6) Fee, C. *Curr. Opin. Chem. Eng.* **2017**, *18*, 10-15.
(7) Fee, C.; Nawada, S.; Dimartino, S. *J. Chromatogr. A* **2014**, *1333*, 18.
(8) Nawada, S.; Dimartino, S.; Fee, C. *Chem. Eng. Sci.* **2017**, *164*, 90-98.
(9) Lottes, F.; Arlt, W.; Minceva, M.; Stenby, E. H. *J. Chromatogr. A* **2009**, *1216*, 5687-5695.
(10) Salmean, C.; Dimartino, S. *Chromatographia* **2019**, *82*, 443-463.
(11) Schure, M. R.; Maier, R. S.; Kroll, D. M.; Davis, H. T. *Anal. Chem.* **2002**, *74*, 6006-6016.
(12) Li, L.; Yan, X.; Yang, J.; Wang, Q. *Appl. Energy* **2017**, *185*, 2168-2180.
(13) Schure, M. R.; Maier, R. S. *J. Chromatogr. A* **2018**, *1580*, 30-48.
(14) Nawada, S.; Dimartino, S.; Fee, C. J.; International Labmate, 2014.
(15) Reider, M. B.; Sterling, J. D. *Comput. Fluids* **1995**, *24*, 459-467.
(16) Pan, C.; Luo, L.-S.; Miller, C. T. *Comput. Fluids* **2006**, *35*, 898-909.
(17) Perko, J.; Patel, R. A. *Phys. Rev. E: Stat. Phys., Plasmas, Fluids,* **2014**, *89*, 053309.
(18) Cohen, Y.; Metzner, A. B. *AlChE J.* **1981**, *27*, 705-715.
(19) Shalliker, R. A.; Broyles, B. S.; Guiochon, G. *J. Chromatogr. A* **2000**, *888*, 1-12.
(20) Poole, C. F. *The Essence of Chromatography*; Elsevier, 2003.
(21) de Wolff, P. M.; Belov, N. V.; Bertaut, E. F.; Buerger, M. J.; Donnay, J. D. H.; Fischer, W.; Hahn, T.; Koptsik, V. A.; Mackay, A. L.; Wondratschek, H.; Wilson, A. J. C.; Abrahams, S. C. *Acta Crystallogr. Sect. A: Found. Crystallogr.* **1985**, *41*, 278-280.
(22) Zick, A. A.; Homsy, G. M. *J. Fluid Mech.* **1982**, *115*, 13-26.
(23) Daneyko, A.; Hlushkou, D.; Khirevich, S.; Tallarek, U. *J. Chromatogr. A* **2012**, *1257*, 98-115.
(24) Daneyko, A.; Höltzel, A.; Khirevich, S.; Tallarek, U. *Anal. Chem.* **2011**, *83*, 3903-3910.
(25) Kolev, N. *Packed Bed Columns: For Absorption, Desorption, Rectification and Direct Heat Transfer*; Elsevier Science, 2006.
(26) Ergun, S. *Chem. Eng. Prog.* **1952**, *48*, 89-94.
(27) Kozeny, J. *Über kapillare leitung des wassers im boden:(aufstieg, versickerung und anwendung auf die bewässerung)*; Hölder-Pichler-Tempsky, 1927.
(28) Jin, L.; Zhang, X.-R. *Appl. Therm. Eng.* **2013**, *50*, 1-11.
(29) van Deemter, J. J.; Zuiderweg, F. J.; Klinkenberg, A. *Chem. Eng. Sci.* **1956**, *5*, 271-289.
(30) Bristow, P. A.; Knox, J. H. *Chromatographia* **1977**, *10*, 279-289.
(31) Heftmann, E. *Chromatography: Fundamentals and applications of chromatography and related differential migration methods - Part A: Fundamentals and techniques*; Elsevier Science, 2004.
(32) Darcy, H. *Les fontaines publiques de la ville de Dijon: exposition et application*; Victor Dalmont, 1856.
(33) Song, H.; Adams, E.; Desmet, G.; Cabooter, D. *J. Chromatogr. A* **2014**, *1369*, 83-91.
(34) Bird, R. B.; Stewart, W. E.; Lightfoot, E. N. *Transport Phenomena*; Wiley, 2007.
(35) Gorard, S. *Br. J. Educ. Stud.* **2005**, *53*, 417-430.

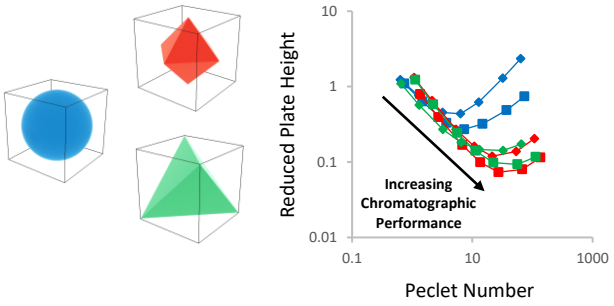

For Table of Contents only